High Deborah Number Flows Through 3D Contractions at the Microscale

M.S.N. Oliveira*, A.M. Afonso*, F. T. Pinho**, M. A. Alves*
*CEFT, Departamento de Engenharia Química, Faculdade de Engenharia da Universidade do Porto, Rua Dr. Roberto Frias, 4200-465 Porto, Portugal. monica.oliveira@fe.up.pt; aafonso@fe.up.pt; mmalves@fe.up.pt Tel. +351 225081680 Fax +225081449.
**CEFT, Departamento de Engenharia Mecânica e Gestão Industrial, Faculdade de Engenharia da Universidade do Porto, Rua Dr. Roberto Frias, 4200-465 Porto, Portugal. fpinho@fe.up.pt Tel. +351 225081597 Fax +351 225081440.

ABSTRACT

In this work, we report a rich sequence of elastic transitions captured experimentally using a viscoelastic, shear-thinning solution. The experiments were carried out in a microchannel with a sudden contraction followed by a smooth expansion, taking advantage of the distinctive conditions provided by microfluidic viscoelastic flows, i.e the capability of achieving high Deborah numbers (*De*) while keeping the Reynolds numbers low enough so that inertia does not have a significant impact. We studied the effect of *De* on the flow patterns and were able to achieve a flow regime, at sufficiently high *De*, in which the flow becomes unsteady with the main vortices formed upstream of the contraction varying in size substantially and very rapidly resembling what Afonso et al. [1] coined as the back-shedding regime. This process is accompanied by the formation of secondary vortices, which are shed in the upstream flow direction. A similar phenomenon was also captured by our preliminary numerical simulations performed using the Oldroyd-B constitutive equation.

Keywords: viscoelastic fluids, contraction flow, elastic instabilities, flow visualization, finite volume method

1 INTRODUCTION

The flow through sudden contractions is a long-standing problem and has been reported in numerous experimental and numerical works, using both Newtonian and non-Newtonian fluids (cf. [1-9]). There are three main types of configuration used in sudden contraction flow research: axisymmetric, planar 2-D and planar 3-D geometries. The latter are especially relevant at the microscale as many microfabrication techniques yield planar channels of constant depth where wall effects are non-negligible.

In spite of the simple geometry, these flows exhibit complex flow patterns comprising regions of strong shearing close to the walls and nonhomogeneous extension along the centerline near the contraction region [10]. One of the remarkable features of viscoelastic fluid entry flows is the formation and subsequent enhancement of vortices upstream of the contraction plane.

As a consequence of miniaturization, contraction flows at the microscale occur under low Reynolds number (*Re*) conditions corresponding to the laminar flow regime [6,7,10]. Furthermore, the small length-scales and large contraction ratios typical of microfluidics result in high extensional deformation rates and high total extensional strains that typically lead to strong nonlinear flow effects even with dilute and semidilute polymer solutions [6,7,11]. In particular, Rodd et al. [6,7] have studied experimentally the flow of various polyethylene oxide solutions through a 16:1 contraction and have shown a series of inertio-elastic transitions that could not have been observed in equivalent experiments at the macroscale.

In numerical terms, simulations of viscoelastic fluid flows through contractions are notoriously difficult at high Deborah numbers (*De*) and are usually limited to flows below a critical *De*. Above the critical *De* value, the numerical simulations typically present mesh dependency problems (even with refined meshes) and are often not able to obtain a converged solution. Very recently, Afonso et al [1] used a finite volume method with the log-conformation formulation, originally proposed by Fattal and Kupferman [12] that allowed reliable numerical simulations to be extended to much higher Deborah numbers than in previous works. The results of their 2D simulations using the Oldroyd-B constitutive equation, showed that local flow unsteadiness appears at a relatively low Deborah number (*De* = 2.5) and that a subsequent increase in *De* leads a growth of the flow unsteadiness resulting in asymmetric flow with alternate back-shedding of vorticity from pulsating upstream recirculating eddies. Additionally, the authors report a frequency doubling mechanism, which eventually leads to a chaotic regime at high *De*. These numerical results were the motivation for our own experimental work reported here, in which we aim to capture experimentally the same type of flow features and try to understand, aided by numerical simulations, the mechanisms underlying the flow transitions that take place at high Deborah numbers.

2 EXPERIMENTAL METHODS

2.1 Microchannel Geometry and Set-up

The experiments were carried out using microfabricated channels consisting of a sudden contraction followed by a smooth expansion with a nearly-hyperbolic shape. The

geometry is symmetric about the plane $y = 0$ and was fabricated in polydimethylsiloxane, PDMS (Sylgard 184, Dow Corning), from an SU-8 photoresist mold by standard soft-lithography techniques. The geometry produced is planar with a constant depth $h = 45$ μm and is depicted in Fig. 1, where the main variables are identified.

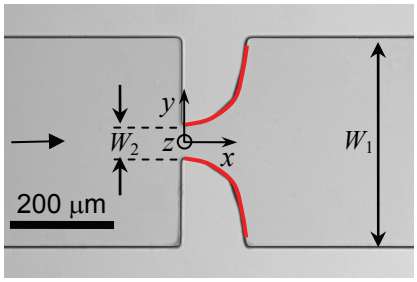

Figure 1. Micrograph of the contraction geometry used in the experiments, where the shape of the quasi-hyperbolic walls are marked in red.

The width of the inlet and outlet channels (W_1) is the same and equal to 400 μm and the expansion region is well defined the following equation:

$$y = \pm 200/[1 + 0.05\,(L^* - x) - 2.5\times10^{-5}\,(L^* - x)^2] \qquad (1)$$

valid for $0 \le x \le L^*$ with $L^* = 123$ μm. The contraction ratio defined as $CR = W_1/W_2$, where W_2 is the projected channel width at the contraction plane, amounts to $CR = 6.4$ for the present geometry.

A syringe pump (Harvard Apparatus PHD2000) was used to control the flow rate at the inlet using syringes with different volumes according to the required flow rate. For the flow visualizations, we used an optical set-up composed of an inverted epi-fluorescence microscope (DMI 5000M, Leica Microsystems GmbH) fitted with an appropriate filter cube (Leica Microsystems GmbH, excitation BP 530–545 nm, dichroic mirror 565 nm, barrier filter 610–675 nm). The flow patterns were captured by streak photography (with *long* exposures) using a CCD camera (Leica Microsystems GmbH, DFC350 FX), and a 100W mercury lamp as illumination source. For this purpose, the fluid was seeded with 1 μm fluorescent tracer particles (Nile Red, Molecular Probes, Invitrogen, Ex/Em: 520/580 nm).

All images shown in this work were captured at the center plane of the geometry using a 20× (NA = 0.25) microscope objective (Leica Microsystems GmbH). For the set-up used, the depth of field corresponds to $\delta z = 4.55$ μm calculated according to:

$$\delta z = \frac{n\lambda_0}{(\mathrm{NA})^2} + \frac{ne}{(\mathrm{NA})M} \qquad (1)$$

where n is the refractive index, λ_0 is the wavelength of the light (in vacuum), NA is the numerical aperture of the objective, e is the minimum detectable size and M is the total magnification (in this case $e/M = 0.65$ μm).

2.2 Fluid Rheology

The viscoelastic fluid used in the experiments is a solution of polyethylene oxide (PEO, with a molecular weight $M_w = 8\times10^6$ g mol^{-1} supplied by Sigma-Aldrich) in a water/glycerol mixture prepared using a magnetic stirrer at low speeds, in order to prevent unnecessary mechanical degradation of the polymer molecules. The composition (by weight) is 0.4% PEO, 66.3% water and 33.3% glycerol.

The fluids were characterized rheologically using a rotational rheometer (Anton Paar, Physica MCR301) and capillary break-up extensional rheometer (Haake CaBER 1, Thermo Scientific). The latter is employed to quantify the response of the fluid to an extensional deformation. In particular, a liquid bridge confined between the two plates (of diameter $D_p = 6$ mm) is stretched as the top plate moves (-50 ms $\le t \le 0$) from an initial ($h_i = 3$ mm) to a final height ($h_f = 12$ mm) and the subsequent evolution of the filament diameter is monitored using a laser micrometer. In the regime when surface tension and elasticity govern the filament drainage the local extensional rate in the filament is constant and the diameter of the filament (D) decays exponentially with time (t) according to [13]:

$$D(t)/D_p \propto \exp[-t/(3\lambda)] \qquad (2)$$

The filament thinning evolution of the PEO solution is shown in Fig. 2 and the fit of Equation (2) to the region of exponential decay is shown in red, yielding a relaxation time $\lambda = 123$ ms.

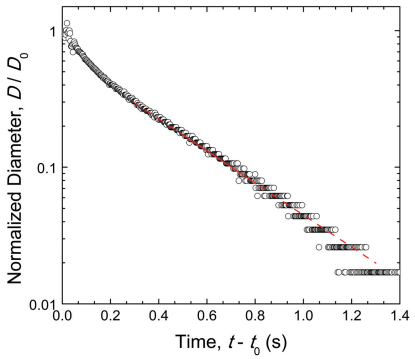

Figure 2. Filament thinning obtained during a CaBER experiment (only part of the experimental data is plotted to improve visually the figure).

The steady-shear viscosity measurements were carried out at 20ºC for a range of shear rates ($1 \le \dot{\gamma}\ /\mathrm{s}^{-1} \le 10\,000$) using a cone and plate geometry (50 mm in diameter and 1º angle) and are shown in Fig. 3a. In Fig. 3b, we illustrated the storage and loss moduli (G' and G'') in dynamic shear flow. The fluid exhibits a shear thinning behavior, as a result of shear induced changes in the microstructure - as

the shear rate is increased, the polymer molecules orient and align with the flow direction.

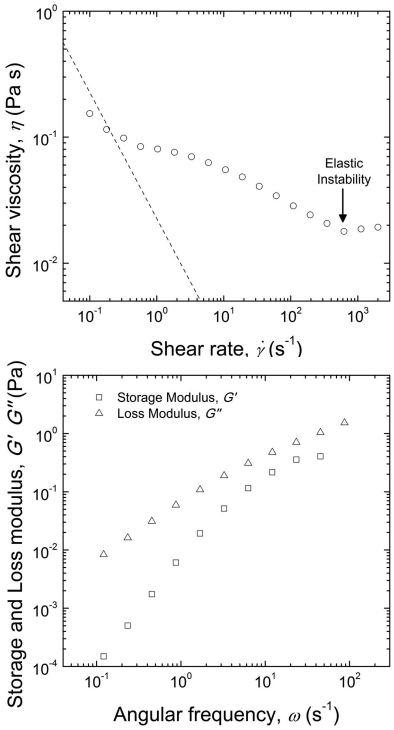

Figure 3. Rheological characteristics of the fluid: (a) Steady-shear flow curve; (b) Dynamic shear data measured under small amplitude oscillatory shear (SAOS) flow.

3 NUMERICAL METHOD AND GOVERNING EQUATIONS

The equations we need to solve are those of conservation of mass and momentum:

$$\nabla \cdot \mathbf{u} = 0 \tag{3}$$

$$\rho \frac{\partial \mathbf{u}}{\partial t} + \rho \nabla \cdot \mathbf{uu} = -\nabla p + \nabla \cdot \boldsymbol{\tau} + \eta_s \nabla^2 \mathbf{u} \tag{4}$$

together with an appropriate constitutive equation for the extra stress tensor. Here we use the Oldroyd-B model:

$$\boldsymbol{\tau} + \lambda \left(\frac{\partial \boldsymbol{\tau}}{\partial t} + \nabla \cdot \mathbf{u}\boldsymbol{\tau} \right) = \eta \left(\nabla \mathbf{u} + \nabla \mathbf{u}^{\mathrm{T}} \right) + \lambda \left(\boldsymbol{\tau} \cdot \nabla \mathbf{u} + \nabla \mathbf{u}^{\mathrm{T}} \cdot \boldsymbol{\tau} \right) \tag{5}$$

A fully-implicit finite-volume method was used to solve Equations (3) – (6). The numerical technique has been described in detail elsewhere [14-16] and is not repeated here due to space restrictions.

4 RESULTS AND DISCUSSION

The effect of the Deborah number on the flow patterns captured experimentally was studied by varying the flow rate imposed using the syringe pump. For very low flow rates, the flow resembles that obtained under Newtonian creeping flow conditions (Fig. 4a), and an increase in the flow rate leads to the formation and growth of symmetric lip (Fig. 4b) and (later) corner vortices (Fig. 4c) upstream of the contraction as observed previously in sudden and smooth contractions with dilute polymer solutions [2]. This is followed by an asymmetric steady flow region, in which the two vortices exhibit slightly different sizes; eventually, as the flow rate is increased further, the flow becomes unsteady and the main vortices pulsate, growing and shrinking slightly in a periodic fashion (Fig. 4d). At sufficiently high Deborah numbers, this process becomes more dramatic and resembles what Afonso et al. [1] coined as back-shedding regime in which the size of the main vortices varies substantially and very rapidly (Fig. 4e), a process accompanied by the formation of upstream secondary vortices, which are shed in the upstream flow direction (Fig. 4e). This time dependent behavior including the formation and shedding of upstream secondary vortices was also captured by our numerical simulations with 2D meshes using the Oldroyd-B model (Fig. 5). Although the experimental and numerical results are not in quantitative agreement, the results are encouraging and we expect that using a more suitable constitutive equation (eg. PTT model) and 3D calculations will be able to provide more realistic predictions.

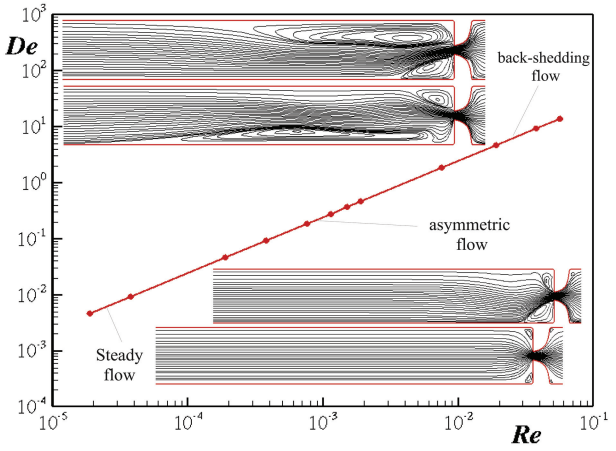

Figure 5. Numerically obtained flow map on the *De* - *Re* parameter space.

Acknowledgements

The authors would like to acknowledge financial support of FCT through projects REEQ/262/EME/2005, REEQ/928/EME/2005, PTDC/EME-MFE/099109/2008 and scholarship SFRH/BPD/75436/2010.

REFERENCES

[1] A.M. Afonso, P.J. Oliveira, F.T. Pinho and M.A. Alves, Numerical study of entry flows of viscoelastic fluids, J. Fluid Mech., 2011 (in press).
[2] D.V. Boger, Ann. Rev. Fluid Mech., 19, 157, 1987.
[3] S.A. White, A.D. Gotsis and D.G. Baird, J Non-Newt. Fluid Mech., 24, 121, 1987.

[4] J.P. Rothstein and G.H. McKinley, J. Non-Newt. Fluid Mech., 98, 33, 2001.
[5] M.A. Alves, F.T. Pinho and P.J. Oliveira, AIChE J., 51, 2908, 2005.
[6] L.E. Rodd, T.P. Scott, D.V. Boger, J.J. Cooper-White and G.H. McKinley, J. Non-Newt. Fluid Mech., 129, 1, 2005.
[7] L.E. Rodd, J.J. Cooper-White, D.V. Boger and G.H. McKinley, J. Non-Newt. Fluid Mech., 134, 170, 2007.
[8] M.S.N. Oliveira, P.J. Oliveira, F.T. Pinho and M.A. Alves, J. Non-Newt. Fluid Mech., 147, 92, 2007.
[9] P.C. Sousa, P.M. Coelho, M.S.N. Oliveira and M.A. Alves, J. Non-New. Fluid Mech., 160, 122, 2009.
[10] M.S.N. Oliveira, L.E. Rodd, G.H. McKinley and M.A. Alves, Micro Nanofluidics, 5, 809, 2008.
[11] C.J. Pipe and G.H. McKinley, Mech. Res. Comm., 36, 110, 2009.
[12] R. Fattal and R. Kupferman, J. Non-Newt. Fluid Mech., 126, 23, 2005.
[13] V.M. Entov and E.J. Hinch, J. Non-Newt. Fluid Mech., 72, 31, 1997.
[14] P.J. Oliveira, F.T. Pinho and G.A. Pinto, J. Non-Newt. Fluid Mech, 79, 1, 1998.
[15] M.A. Alves, P.J. Oliveira and F.T. Pinho, Int. J. Num. Methods in Fluids, 41, 47, 2003.
[16] A.M. Afonso, P.J. Oliveira, F.T. Pinho and M.A. Alves, J. Non-Newt. Fluid Mech., 157, 55, 2009.

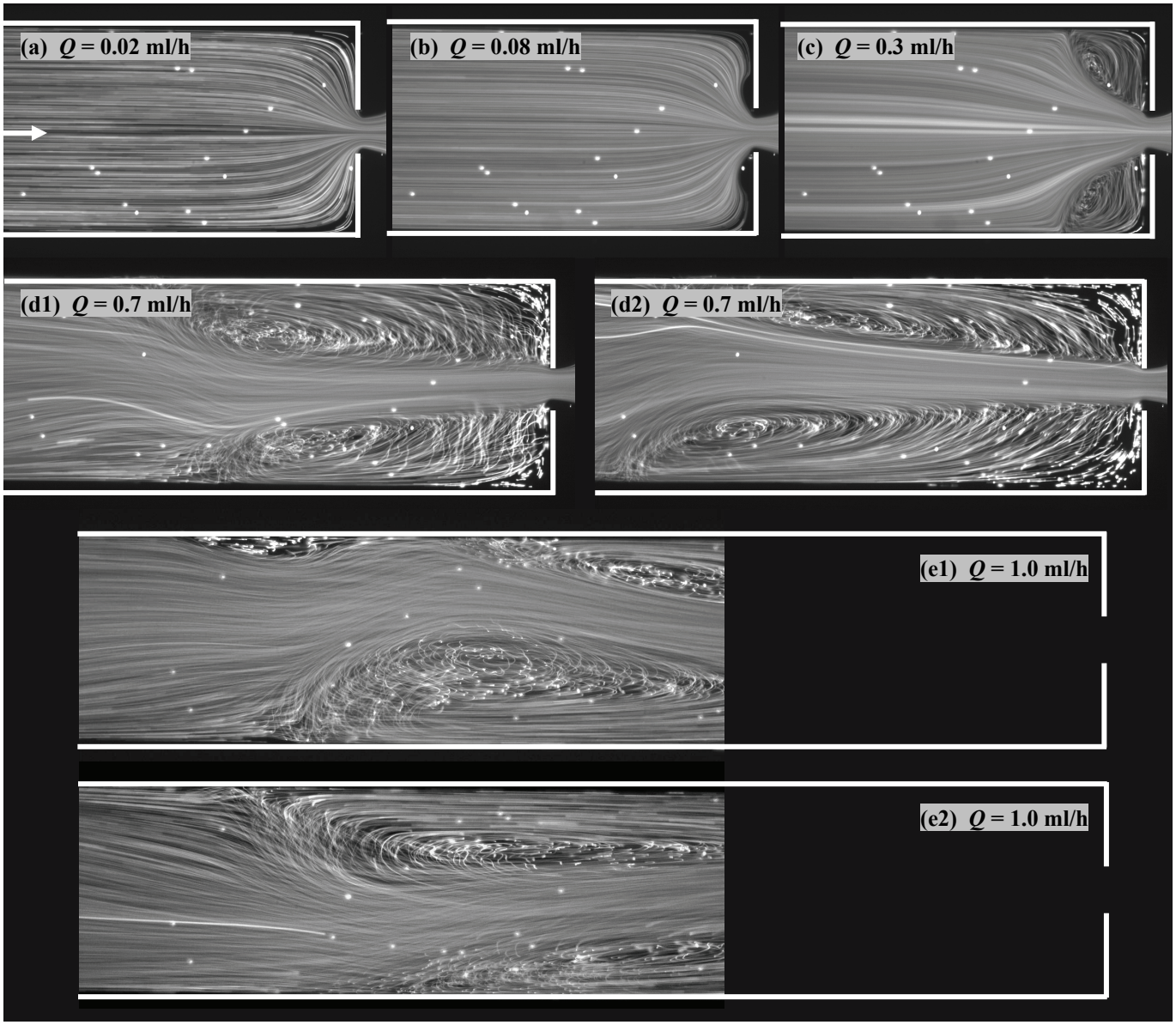

Figure 4. Effect of the flow rate on the flow patterns obtained experimentally. For Q = 1.0 ml/h the images were captured further upstream of the contraction and as such the contraction region is not visible. The white lines were drawn to indicate the boundary walls of the microchannel.